



HAL
open science

Incorporation of clusters of titanium oxide in Beta zeolite structure by a new cold TiCl₄-plasma process: physicochemical properties and photocatalytic activity

Mohamad El-Roz, Louwanda Lakiss, Jaafar El Fallah, Oleg Lebedev, Frederic Thibault-Starzyk, Valentin Valtchev

► **To cite this version:**

Mohamad El-Roz, Louwanda Lakiss, Jaafar El Fallah, Oleg Lebedev, Frederic Thibault-Starzyk, et al.. Incorporation of clusters of titanium oxide in Beta zeolite structure by a new cold TiCl₄-plasma process: physicochemical properties and photocatalytic activity. *Physical Chemistry Chemical Physics*, 2013, 15 (38), pp.16198. 10.1039/C3CP52478G . hal-01963797

HAL Id: hal-01963797

<https://hal.science/hal-01963797v1>

Submitted on 5 Oct 2021

HAL is a multi-disciplinary open access archive for the deposit and dissemination of scientific research documents, whether they are published or not. The documents may come from teaching and research institutions in France or abroad, or from public or private research centers.

L'archive ouverte pluridisciplinaire **HAL**, est destinée au dépôt et à la diffusion de documents scientifiques de niveau recherche, publiés ou non, émanant des établissements d'enseignement et de recherche français ou étrangers, des laboratoires publics ou privés.

Cite this: DOI: 10.1039/c0xx00000x

www.rsc.org/xxxxxx

ARTICLE TYPE

Incorporation of clusters of titanium oxide in Beta zeolite structure by new cold TiCl₄-plasma process: physicochemical properties and photocatalytic activity.

Mohamad El-Roz,^{a*} Louwanda Lakiss^a, Jaafar El Fallah^a, Oleg I. Lebedev^b, Frederic Thibault-Starzyk^a,
Valentin Valtchev^a

Received (in XXX, XXX) Xth XXXXXXXXX 20XX, Accepted Xth XXXXXXXXX 20XX

DOI: 10.1039/b000000x

A new post-synthetic approach, involving cold plasma treatment, was employed for the preparation of Ti-Beta zeolite. Zeolite Beta nanoparticles were first subjected to plasma induced deposition of TiCl_y (with $y \leq 3$), which were further converted into TiO_x (with $x \leq 2$) upon O₂-plasma treatment. Different steps of the new elaborated plasma approach were monitored by in situ FTIR spectroscopy. D₂O isotopic exchange was used in order to shed light on the formation of Si-O-Ti bonds induced by TiCl₄-plasma followed by O₂-plasma treatments. The obtained Ti-Beta materials were studied by a set of complementary characterization techniques including FTIR, TEM, SEM-EDS, XRD, N₂ sorption, NMR and UV-Vis techniques. The silanol content and the acidic properties of Ti-Beta composites were also studied. The elaborated materials were tested as photocatalysts for methanol photooxidation in gas phase. Ti-Beta presents a methanol photooxidation rate 8 times higher than a conventional P25-TiO₂ catalyst under UV irradiation.

Introduction

Over the last few years photocatalytic processes using titanium dioxide (TiO₂) as photocatalyst have attracted special interest due to their numerous applications in water and air purification. Because of its high activity and stability, low cost and non toxic nature, titanium dioxide is considered as a very promising photocatalyst. When exposed to light in the presence of oxygen, it produces highly oxidative radical species that successfully oxidize most of the organic pollutants present in air and water into inert ultimate products such as CO₂ and H₂O.

Despite these valuable properties, the use of TiO₂ for industrial purposes remains limited due to the photocharge recombination and adsorption/desorption processes of the reactants and reaction products [8]. It has also been reported that particle size distribution and dispersion of titanium dioxide particles have a direct impact on the efficiency of the catalyst. In this context, researches focused mostly on the deposition of titanium dioxide onto different types of support not only to respond to the needs of highly dispersed TiO₂ nanostructures but also to exploit the adsorption properties of supports that might improve the photocatalytic activity. Several groups reported the preparation of TiO₂ supported onto different types of adsorbents such as fiber glass [9-10], natural fiber [11], activated charcoal [12-13], alumina, silica or zeolite materials.[14-20] Among these supports, zeolites were found to be the ideal candidate due to their high specific surface area and micropore channels that provide confined space for stereoselective reactions. In addition, the

physicochemical properties of zeolitic materials can be easily modified either by in situ or by post-synthesis methods. They are also eco-friendly and their tunable hydrophobic/hydrophilic character provides selective exclusion of undesired molecules or ions [21, 22]. Recent studies have demonstrated the promising photocatalytic efficiency of TiO₂/zeolite composites [17, 23-25] and interesting photovoltaic applications of clusters of titanium dioxide encapsulated within zeolites [26].

TiO₂/zeolite supported photocatalysts can be prepared by different methods that are classified into three main groups: (i) solid state dispersion methods (SSD) or mechanical mixing; [17, 27-29] (ii) post-synthetic approaches as dealumination, followed by a vapor-thermal treatment using a TiO₂ precursor [30]; and (iii) in situ synthesis approaches where TiO₂ nanoparticles are anchored at the zeolite surface during the hydrothermal treatment [14-16].

Plasma treatment (thermal and non thermal) has also been used to prepare nanosized TiO₂ supported thin films (silica wafer, glass wafer...) [31-34]. The most often employed TiO₂ precursor, for this treatment, is the titanium tetraisopropylat that is delivered in gas phase comprising O₂, O₂/Ar, O₂/H₂O [31-34]. As known, during the plasma ionization of an oxygen-containing gas phase, oxidative species (O₂⁺, O, O₃...) are generated. These species are able to oxidize the titanium precursor into crystalline TiO₂ that is deposited on the surface of the support. The formation of relatively large TiO₂ particles limits the preparation of efficient TiO₂/zeolite composites because of the difficulty to incorporate TiO₂ in zeolite pore system.

The present work reports the use of a modified cold TiCl₄-plasma

approach that allows an efficient incorporation of clusters of titanium dioxide in the pore system and on the surface of zeolite-type materials. In contrast to the traditional plasma treatment described above, the present approach consists in the incorporation of atomic scale titanium species in zeolite channels. It is based on a direct-decomposition of the titanium vapor precursor (TiCl_4), by plasma (TiCl_4 -plasma) in absence of any other carrier gas, at low pressure (<0.5 mbar) and at relatively low temperature (<350 K). After the TiCl_4 -plasma process, an O_2 -plasma treatment is performed in order to oxidize the already deposited titanium species that are anchored to zeolite structure favoring then the TiO_x formation by generating high oxidant species [35]. The elaborated TiO_x supported catalysts (Ti-Beta) were subjected to detailed characterization prior to be tested as photocatalysts for methanol photooxidation. For comparison, a reference sample prepared by SSD method (TiO_2/Beta) was employed.

Experimental part

Synthesis and post synthesis treatment

Zeolite Beta synthesis: Nanosized Beta crystals (Beta) were synthesized from a colloidal precursor suspension having the following chemical composition: $0.35 \text{ Na}_2\text{O} : 4.5 (\text{TEA})_2\text{O} : 1 \text{ Al}_2\text{O}_3 : 30 \text{ SiO}_2 : 295\text{H}_2\text{O}$. The silica source for the preparation of the initial precursor suspension was freshly freeze-dried colloidal silica Ludox SM 30 (30 wt %). Aluminium isopropoxide (98%, Aldrich) was used as an alumina source and tetraethylammonium hydroxide (TEAOH, 20 wt% in water, Merck) as a structure-directing agent. These components were mixed under vigorous stirring for 15 min and aged on an orbital shaker at ambient temperature for 24 h prior to the hydrothermal treatment performed at 373 K for 8 days. The nanosized crystals resulting from the hydrothermal treatment of the colloidal suspension were purified by three steps centrifugation (20,000 rpm, 60 min), decanting of the supernatant and redispersion in distilled water using an ultrasonic bath. The resulting suspension was freeze-dried to recover the sample in a powder form. The Beta zeolite crystals were then calcined to remove the organic template. The calcination process consisted in heating the sample from RT to 823 K with a heating rate of 1.75 K/min, kept at 823 K for 5 hours and then cooled down to room temperature in 5 hours.

Preparation of Ti-Beta: The incorporation and encapsulation of titanium oxide in calcined Beta zeolite was performed using a plasma process in a Pyrex reactor (dielectric barrier discharge plasma with a 50 Hz sinusoidal power supply (2 kV)) (Scheme 1-A). After introducing the powder in the reactor, the system was evacuated until the pressure stabilizes at $\sim 10^{-2}$ mbar. Then TiCl_4 was introduced under continuous vacuum in order to reach an equilibrium pressure close to 0.5 mbar in order to purge the plasma reactor. The cold plasma was then turned on to decompose the TiCl_4 precursor in absence of any other gas. It was maintained about 5 to 10 seconds and then the valve of TiCl_4 tube was closed in order to remove the excess of TiCl_4 and the different species formed during plasma. The process was repeated

three times.

It should be noted that in our conditions the plasma was shut-off when the partial pressure of TiCl_4 exceeded 0.7 mbar. The TiCl_4 -plasma treatment was followed by O_2 -plasma treatment for more than 10 minutes (depending of the sample amount) at low pressure (3.5 mbar). During the experiments, the temperature increase due to plasma process up to 393 K. The obtained material was named "Ti-Beta".

For comparison three types of samples were also investigated as references: a TiO_2 sample (P25 from Degussa), an initial zeolite Beta sample (used for the preparation of Ti-Beta), and a TiO_2/Beta (15/85 wt. %) prepared by Solid State Dispersion method using ethanol as solvent.

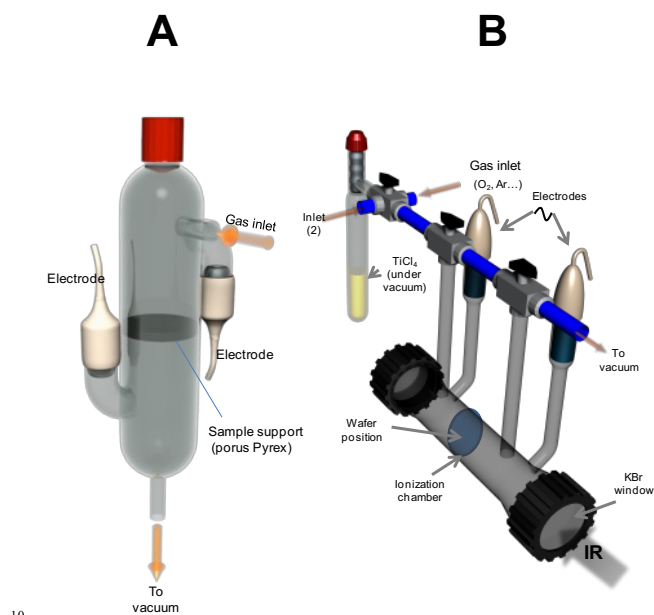
Characterization

In order to investigate the crystallinity and phase purity of the samples, calcined and treated Beta-type crystals were subjected to X-ray diffraction (XRD) analysis using a PAN analytical (X-Pert Pro) diffractometer with $\text{CuK}\alpha_1$ source ($\lambda=0.15406$ nm, 40 kV, 30 mA). The morphological features and the chemical analyses of the samples were studied using Scanning Electron Microscope (SEM, Hitachi S3460) equipped with an energy dispersive spectroscopy (EDS, ThermoNoran) device. Beta and Ti-Beta materials were also characterized by transmission electron microscopy (TEM), including electron diffraction (ED), high resolution TEM (HRTEM) and energy dispersive x-ray (EDX) analysis, using a Technai G2 30UT microscope equipped with an EDAX X-ray microanalysis unit, operating at 300 kV and having 0.17 nm point resolution. The TEM samples were prepared by dispersing the powder onto a copper grid coated with a holey carbon film using ethanol as solvent. Low intensity beam conditions were applied for TEM measurements in order to minimize the degradation and amorphisation of the material under the electronic beam.

Nitrogen sorption measurements were carried out at 77K on a Micromeritics ASAP 2020 after degassing at 423 K for 24 h. The surface areas were calculated using BET equation and the total pore volumes of the samples were estimated at a relative pressure of 0.99. The samples were also investigated by solid state NMR spectroscopy. MAS ^{29}Si and CP MAS $^1\text{H} \rightarrow ^{29}\text{Si}$ NMR experiments were conducted at 300K on a BRUKER ADVANCE 400 DSX spectrometer operating at 400 MHz–9.4 T for the ^1H Larmor frequency, and equipped with a BRUKER 4 mm $^1\text{H}/\text{X}$ solid-state CP MAS probe. A representative sample (~ 50 mg) was placed in a 4-mm zirconium rotor. The Magic-angle spun at 14 kHz with pulse duration of 3.5 ms, contact time of 6 ms and relaxation time of 1s. The number of scans was adjusted to ensure a signal-to-noise ratio of at least 1024. For MAS ^{27}Al NMR experiments, the spectra were recorded with a spinning speed of about 12 kHz. Chemical shifts were referenced to a 0.1 M $\text{Al}(\text{NO}_3)_3$ aqueous solution.

In order to investigate the surface modification of Beta-type zeolite during plasma treatment, in situ FTIR spectroscopy was performed on self-supporting wafers ($20 \text{ mg}/2 \text{ cm}^2$) placed in an in situ FTIR-plasma reactor (Scheme 1-B). First, the pellet was subjected to evacuation under vacuum in order to evacuate the atmospheric gas present in the ionization chamber and to remove water weakly adsorbed on Beta surface. The first dose of TiCl_4 was introduced by opening the valve for ~ 10 s to reach a pressure

of ~0.50 mbar under evacuation. This step allowed the purge plasma reactor from the residual gases that could remained. The IR/plasma experiment was performed in the same order described above (see “post synthesis treatment” part) but for a shorter time due to the low amount of sample (pellet mass ~20 mg). The IR spectra were collected in transmission mode on a Bruker Vertex 80v equipped with a cryogenic MCT detector (4 cm⁻¹ resolution, 8 scans, and acquisition time ~1.2 s).



Scheme 1. Plasma (A) and in situ FTIR-plasma (B) reactors.

The acidic properties of the resulting materials were investigated by IR using pyridine as probe molecule. Powders were pressed (~10⁷ Pa) into self-supported discs (2 cm² area, ~20 mg) and placed in an IR cell equipped with KBr windows. IR spectra were recorded using a Nicolet 6700 IR spectrometer equipped with a MCT detector and an extended-KBr beam splitter was used. Spectra were recorded in the 400-5500 cm⁻¹ range at a resolution of 4 cm⁻¹ and 128 scans were collected for each spectrum. A movable quartz sample holder allowed placing the self-supported discs in the infrared beam, for recording spectra, and moving it into a furnace at the top of the cell for thermal treatment. Pyridine (Py) adsorption was performed by introduction of doses inside the infrared cell containing the previously activated (under vacuum at 473 K for 5 h) self-supported discs of the samples. After introduction of each dose of Py, the Beta sample was heated at 473 K for 10 min to allow diffusion toward all accessible sites before recording spectrum. Infrared spectra were recorded after Py saturation (1.33 mbar at equilibrium) followed by evacuation at 473 K to remove physisorbed species. In all experiments, analytical grade pyridine (Aldrich) was used after water trapping with molecular sieve 3A. The decomposition of the massif into overlapping IR bands of adsorbed pyridine on acidic sites and the calculation of the IR band area have been performed using Omnic v8.2 software. The values were normalized for the same weight

(20 mg) of pellets.

The accessible silanol sites were exchanged with heavy water vapor (D₂O) (10 mbar at equilibrium followed by an evacuation under vacuum at RT). This process was repeated 3 times in order to obtain a total H-D exchange of all accessible silanol sites. After exchange and evacuation, IR measurements were performed on a Nicolet 6700 IR spectrometer equipped with a MCT. Spectra were recorded at 4 cm⁻¹ and 128 scans were co-added for each spectrum.

Photocatalytic tests

In order to test the photocatalytic activity of Ti-Beta materials, photocatalytic oxidation of methanol was performed. Ti-Beta catalyst was pressed into self-supported wafers (2 cm², m~20 mg) and put in the photocatalysis reactor. It was made of a stainless steel cylinder that carries a toroidal sample holder in its centre, where the catalyst self supporting wafer was placed. Tightness was obtained by Kalrez® O-rings, and the dead volume (typically defined as the residual space between each sample face and the windows) was reduced to about 0.4 ml by filling the empty space with KBr windows placed on each side of the sample holder. The photocatalytic system was connected to a flow set-up. Gases were introduced into the lines (heated at 333 K) by mass flow controllers. The system allows the two gas mixtures, so called “activation” and “reaction” flows, to be prepared and sent independently to the reactor cell. Gases were introduced to the sample by 1/8" OD pipe and collected on the opposite side of the sample holder. More details can be found in references [36-38]. For this specific photocatalytic oxidation study, UV irradiation was carried out with a polychromatic light of a Xe-Hg lamp (LC8 spot light Hamamatsu, L10852, 200 W) with UV-intensity about 6 mW/cm² at λ=366nm. It was performed using a UV-light guide (A10014-50-0110) fixed at the entrance of a modified operando cell. The reaction temperature has been maintained at about 298 K.

The low partial pressure of methanol was established using a saturator at controlled temperature. The gas mixture composition was then fixed at 1 vol. % methanol and 20 vol. % O₂ diluted in Ar and the total flow was adjusted to 25 cm³/min. The analysis of the outlet gases was performed by means of a Pfeiffer Omnistar mass spectrometer. P25-TiO₂ has been used as reference in the same condition. Methanol conversion and CO₂-selectivity has been calculated using the m/z=31 and m/z=44 MS signals, respectively [37].

Results and discussion

The as-synthesized zeolite Beta and Ti-Beta composite obtained by plasma treatment are characterized by XRD (Figure 1). Both display relatively broad Bragg reflections peaks characteristic of zeolite Beta structure, built of BEA and BEB polymorphs. No noticeable changes in the structure of the zeolite have been observed after plasma treatment. However, new broad peaks appear in the two theta regions 23-26° and 45-50°. They correspond to TiO₂ anatase phase formed on the Beta surface.

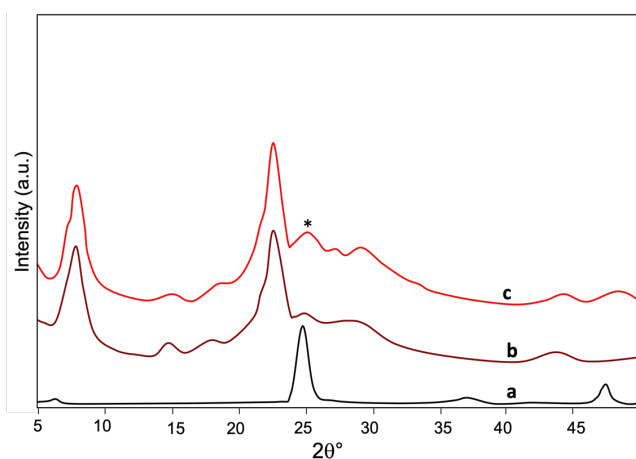


Fig. 1 XRD of pure anatase TiO₂ (a), Beta zeolite (b) and Ti-Beta (c) samples. Note: *Peak assigned to anatase phase.

The titanium content in Ti-Beta sample was determined by EDS and ICP analysis. Figure 2, presents the EDS spectrum of Ti-Beta sample. It displays two peaks at 4.5 eV and 4.8 eV. According to the literature, these two peaks are assigned to K_{α1} and K_β of titanium, respectively [40]. According to ICP results, the Si/Al ratio increases of about 5% after plasma treatment from Si/Al=20.1 to 21.2. This result shows a partial extraction of Al from zeolite structure after plasma treatment. The amount of Titanium species introduced is estimated to 11 wt %. Besides, the cartography measurements performed on the composite Ti-Beta sample and the mechanical mixture TiO₂/Beta (15/85 % wt.) show clearly the higher dispersion of Ti atoms in the Ti-Beta structure in respect to TiO₂/Beta (Figure S1 in supplementary information).

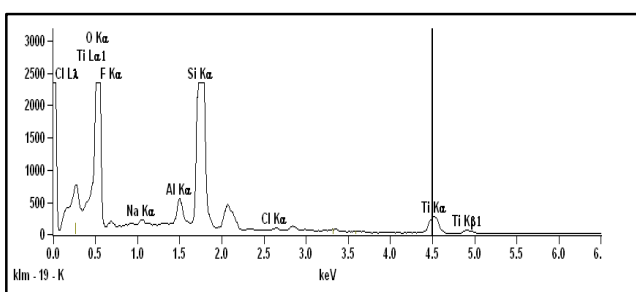


Fig.2 EDS spectrum of Ti-Beta sample.

In order to determine the textural properties of calcined Beta, Ti-Beta, TiO₂/Beta and P25-TiO₂ samples, nitrogen sorption analysis was performed. Table 1 summarizes the most important characteristics of these materials. As shown at Figure 3, all zeolite containing samples display a typical type I isotherm with hysteresis loops at high relative pressure. This latter is related to the textural porosity of aggregated nanosized zeolite crystals. The microporous volume was found to decrease in the following order Beta > TiO₂/Beta > Ti-Beta. The specific surface area decreased as well in the same order 635, 570 and 420 m² g⁻¹ for Beta, TiO₂/Beta and Ti-Beta, respectively. The decreasing of the

specific surface area and microporous volume of SSD prepared sample TiO₂/Beta is obviously due to the presence of 15 wt % bulk TiO₂. Although, Ti-Beta sample contains a close amount (11%) of TiO_x (x≤2) species, a more pronounced decreasing of its microporous volume in respect to TiO₂/Beta was observed. This substantial difference in their microporous volume suggests that some amount of TiO_x species introduced by plasma is located most probably in zeolite channels.

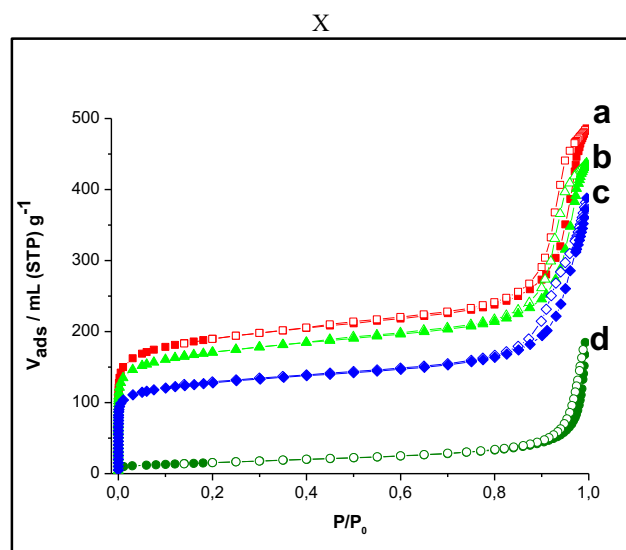


Fig. 3 Nitrogen adsorption (close symbol) and desorption (open symbol) isotherms of initial zeolite Beta (a), SSD prepared TiO₂/Beta (b), Ti-Beta (c) and P25-TiO₂ (d) samples.

Figure 4 shows the ²⁹Si MAS NMR spectra of the initial zeolite Beta and Ti-Beta samples. The two main signals, observed at -112 ppm and -105 ppm, are attributed to Q₄ ((SiO)₄Si) and Q₃ species ((SiO)₃SiOH), respectively. The signal assigned to the ((SiO)₃SiOTi) species, for Ti-Beta materials, appears at a higher field than that of (SiO)₄Si (Q₄), which explain the low resolution of Q₄-Q₃ signals for this sample [41]. As shown at Figure 5, the ²⁷Al MAS NMR spectrum of Ti-Beta shows an increase of the signal at 0 ppm usually attributed to hexacoordinated aluminum species. Such a result reveals a partial dealumination of the structure after plasma treatment (in addition to the 5 wt.% of alumina extracted from the structure and determined by ICP measurement). In addition, ¹H→²⁹Si cross polarization experiments (Figure 4B), that are more sensitive to Si-OH groups, show a spectacular increase of the Q₄/Q₃ ratio after the plasma incorporation of Ti. These results clearly point out a chemical interaction of Ti with the structure of zeolite and suggest the formation of Si-O-Ti bond after TiCl₄-plasma treatment. This process is certainly complex and involves the interaction of chlorine ions with Al species followed by formation of Si-O-Ti linkages. Unfortunately, it is not possible to quantify the number of Aluminum sites substituted since hexacoordinated aluminium species are still present in the zeolite as shown by ²⁷Al mas NMR. But, according to ICP analysis this amount could be estimated to higher than 5%.

Cite this: DOI: 10.1039/c0xx00000x

www.rsc.org/xxxxxx

ARTICLE TYPE

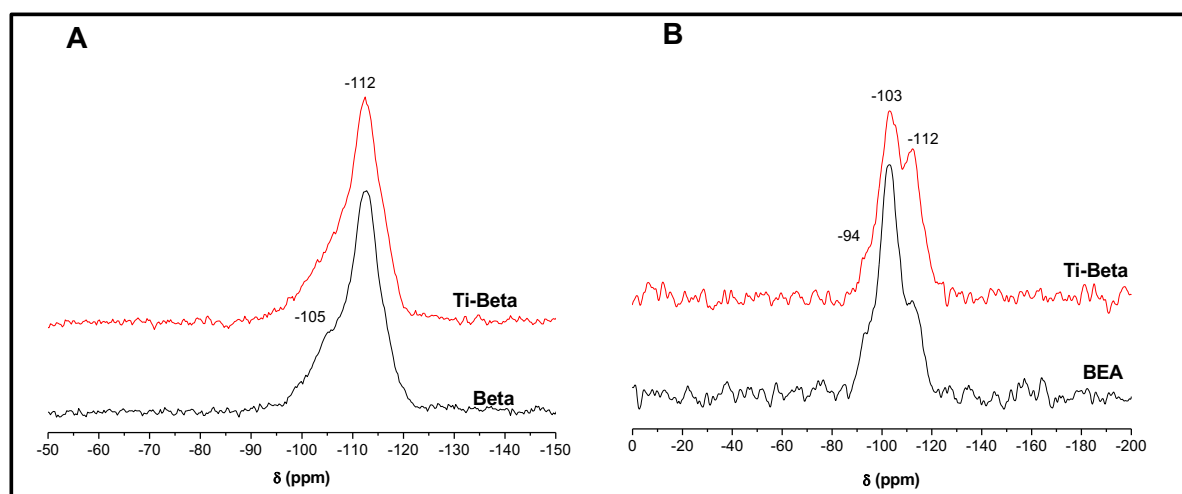


Fig. 4 ^{29}Si MAS NMR (a) and CP MAS $^1\text{H} \rightarrow ^{29}\text{Si}$ (b) NMR spectra of Beta and Ti-Beta samples.

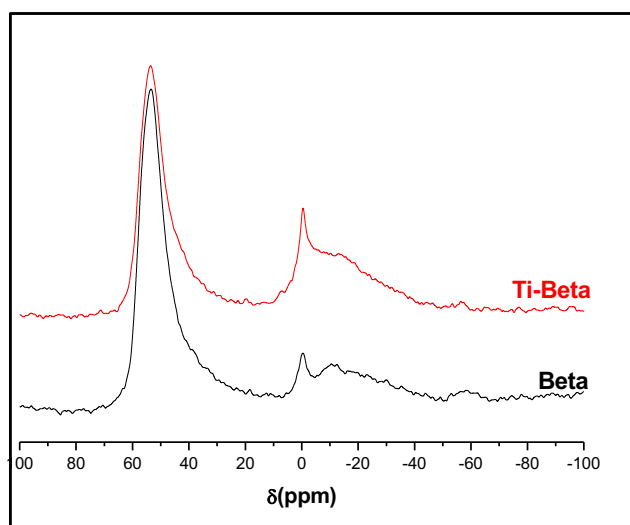


Fig. 5 ^{27}Al MAS NMR spectra of Beta and Ti-Beta samples.

Figure 6 includes the UV spectra of Beta-type material after calcination, Ti-Beta sample, and TiO_2 -p25. The initial Beta-type material exhibits a very low UV absorption. However, titanium-modified Beta material showed substantially different UV absorption characteristics, namely a blue shift of the UV spectra as compared to anatase and rutile forms of TiO_2 . A broad band is observed between 200 and 350 nm, with a maximum centered at ca. 270 nm (Figure 6). It is assigned to a charge transfer between oxygen and Ti atoms, simultaneously present in tetra-, penta- and hexacoordinated species. This band is broader than the one observed in TS-1 zeolite containing namely framework Ti [42,43]. Similar spectrum has been recorded for nanoclusters

titanium oxide on silica [44]. Therefore, the UV spectra reveals the presence of clusters of titanium oxide in Ti-Beta zeolite [42-44]. This result shows also the presence of species with different coordination, including tetrahedral coordination that could be attributed to Ti atoms in zeolite framework.

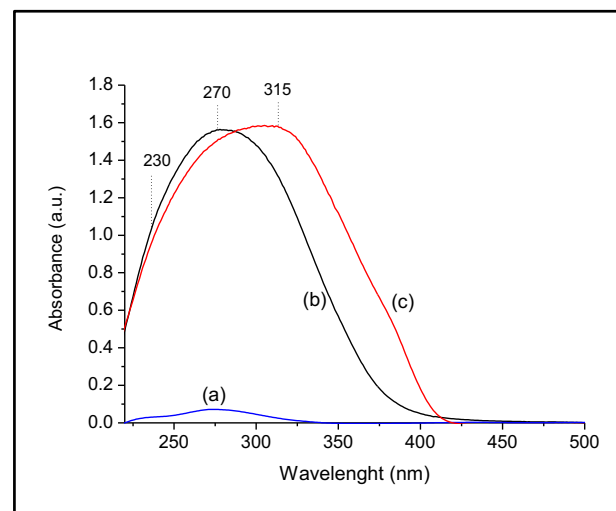


Fig. 6 DR UV-visible spectra of zeolite Beta (a), Ti-Beta (b) and P25- TiO_2 (c).

The bright-field TEM image (Figure S3) shows Beta zeolite nanocrystal with typical size around 100 nm that are randomly surrounded by nanosized particles as it can be seen from at the insert enlarged image. The insert ring ED pattern taken for this crystal shows evidence of coexistence of ultra small size TiO_2 nanoparticles and Beta zeolite crystals. In particular, together with the diffraction spots attributed to Beta zeolite, a faint ring is observed in ED pattern. It corresponds to 3.5 Å which is typical

(011) spacing of TiO₂ anatase structure (ICSD 9852). This result is in agreement with that observed above by XRD.

High resolution TEM (HRTEM) gives more evidence and information on the structure and spatial distribution of TiO₂ nanoparticles. The bright field HRTEM image of single Beta nanocrystal reported at Figure 7 reveals a mixture of small and ultra small nanoparticles in the sample. The size and distribution of bigger particles is particularly clear in Figure 7a and 7d. The small TiO₂ particles have a typical size of 4-6 nm and definitely located at the surface of Beta nanocrystals. The surface of Zeolite nanocrystals is completely covered. Determine the structure and spatial distribution of clusters of TiO₂ by TEM is far from trivial due to the overlapping of the layer of big TiO₂ nanoparticles on the surface and zeolite Beta matrix. However, bright field HRTEM image in Figure 7c shows very small particles with a scale size of 1-2 nm eventually spread, as dark spots, throughout the specimen. Unfortunately it is not possible to determine the

spatial position of Ti-O particles within Beta Zeolite framework due to the two dimensional aspect of TEM images, and even by using electron tomography because of extremely small size, weak contrast and complex structure of Ti-Beta material [45]. Nevertheless, the comparison of HRTEM images of pure Beta zeolite (Figure 7b) and Ti-Beta crystals highlights two important points. The first point concerns the crystal structure: Ti-Beta Zeolite crystals exhibit disordered lattice (Figure 7c) with respect to pure Beta Zeolite crystals (Figure 7b). The second point is that the Ti-O_x nanoparticles appearing as dark contrast spots (marked by white arrows in Figure 2c) exhibit quite uniform size (~2 nm) and shape (square-like) distribution. As the Beta Zeolite consists of cubically arranged pores, it is logical to assume that the nanoparticles should follow this arrangement if they are embedded within the structure framework. Thus according to these evidences, it is reasonable to conclude that cluster of titanium oxide are encapsulated within Beta Zeolite framework.

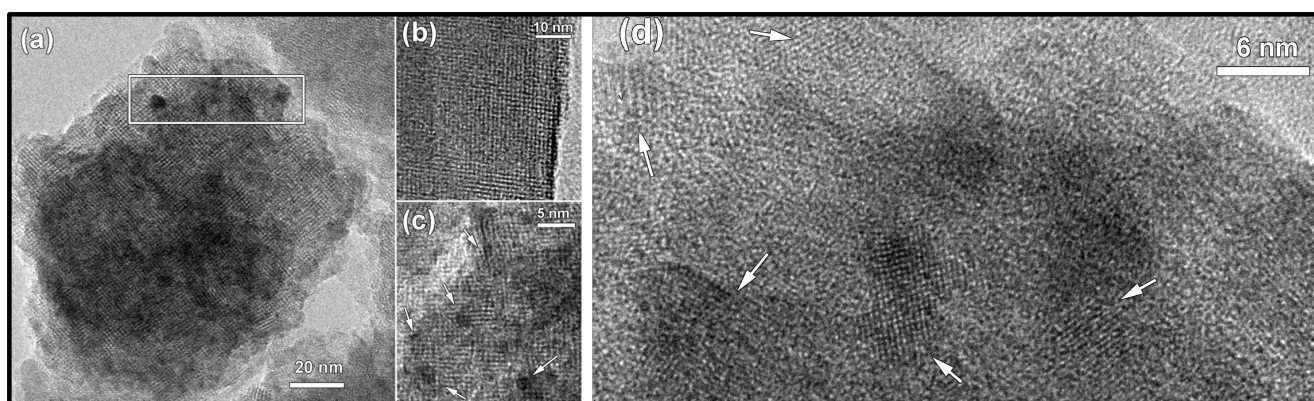


Fig.7 a) Bright field HRTEM image of single Ti-Beta Zeolite crystal; b) bright field HRTEM image of parent Beta zeolite; c) Enlarged HRTEM image of Ti-Beta. The dark spots Ti-O nanoparticles are pointed by white arrows; d) Enlarged image of the region marked in (a). The TiO₂ particles with range size between 4-6 nm are depicted by white arrows.

In situ FTIR-plasma results: The IR spectrum of Beta zeolite sample displays two main narrow bands at 3740 cm⁻¹ and 1630 cm⁻¹ (Figure 8), in addition to the characteristic structural vibration bands. These two bands correspond respectively to the ν(OH) of terminal silanol groups and to the δ(H₂O) of adsorbed water molecules [46-48]. The broad band appearing between 3700 and 2800 cm⁻¹ is assigned to hydrogen bonded terminal silanol groups Si-OH with physisorbed water molecules [46-48]. The evolution of the IR spectra during plasma treatment and after each treatment step is reported at Figure 8-A and Figure 8-B, respectively. First, the introduction of TiCl₄ leads to the disappearance of the band assigned to adsorbed water molecules in Beta zeolite. This is coupled with a decrease of the hydrogen bonding band related with the terminal silanol band. These changes in the IR spectra were assigned to the oxidation of TiCl₄ to Ti(OH)_nCl_(4-n) (n ≤ 3) in the presence of physisorbed water and to the formation of SiOTi(OH)_mCl_(3-m) (m ≤ 3) in the presence of terminal SiOH groups [47]. The total consumption of water molecules, traduced by the complete disappearance of the vibration band of water at 1630 cm⁻¹, shows that all the accessible sites to water were also accessible to TiCl₄. The broad band of SiOH vibration, which is still present, is most probably a consequence of the hydrogen bonding between SiOH sites and

hydrolysed titanium precursor. When TiCl₄-plasma is turned on, a notable decrease of the SiOH bands is observed in the first few seconds. The observed changes are related to TiCl₄ decomposition and generation of active ions and/or radicals (i.e. (TiCl_{4-n})^{m+}, Cl•, Cl⁻...) that favor Si-OH and TiOH condensation to form SiOTi and/or TiOHs condensation to TiOTi bonds. This result is in agreement with the NMR results discussed above. The O₂-plasma treatment results in further condensation and oxidation of the reduced titanium species that could be present in the structure to TiO_x (x ≤ 2). The arising of the narrow band at ~3740 cm⁻¹ after O₂-plasma (Figure 8b-d) can be assigned to inaccessible silanol groups and/or to the formation of terminal TiOH groups after the condensation reaction (TiOH...TiOH...TiOH + oxydant species → TiOTiOTiOH + H₂O).

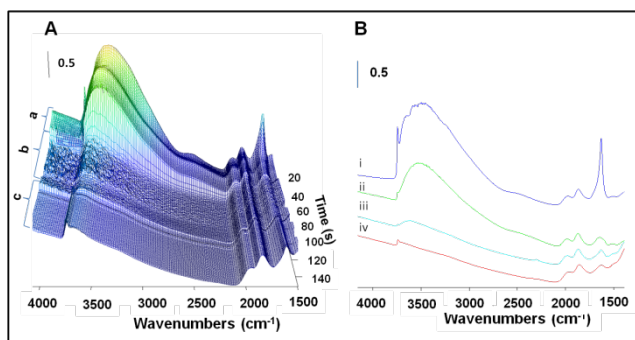


Fig.8 (A) Evolution of zeolite Beta IR spectrum vs the treatment time: during TiCl₄ introduction (a), during TiCl₄-plasma (b) and during O₂-plasma treatment (c). (B) IR spectra of Beta zeolite (i), after TiCl₄ introduction (ii), after TiCl₄-plasma (iii) and after O₂-plasma (iv) treatment.

Silanol content in Ti-Beta and Beta samples: Figure 9 presents the IR spectra of zeolite Beta nanocrystals and Ti-Beta samples in the SiOH vibration region after activation of the parent zeolite Beta samples at 623 K under vacuum for 1 h and after O₂-plasma treatment for Ti-Beta. The silanol contents has been determined using the normalized area of the $\nu(\delta)$ SiOH vibration band at 4570 cm⁻¹ (insert of Figure 8, Table 1) [49]. An important decrease of SiOH groups after TiCl₄-plasma followed by O₂-plasma treatment can be observed (Figure 9, insert). The comparative study revealed that the relative silanol contents in Beta/Ti-Beta samples are equal to 2.4/1. This result unambiguously confirms that more than 50% of silanols defects disappear after TiCl₄-plasma treatment and proves that the extracted Aluminum species were substituted by Ti. The analysis has been repeated several times in order to verify the reproducibility of the result and to estimate the relative incertitude ($\pm 5\%$) on silanol ratio values.

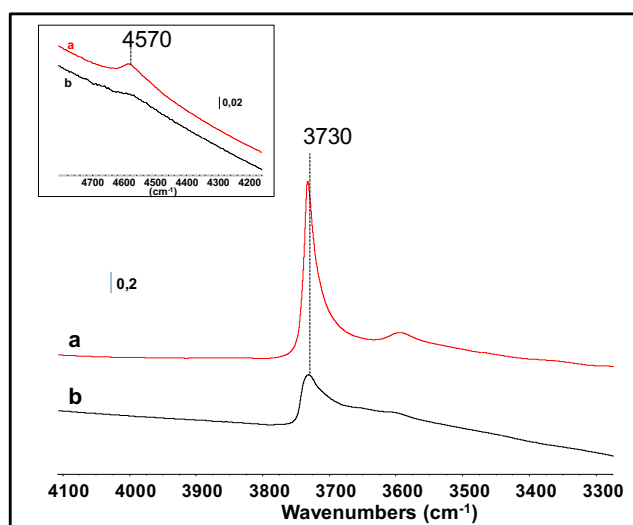


Fig.9 IR spectra of Beta sample after activation at 673 K under vacuum (a) and Ti-Beta sample after plasma treatment in the OH vibration region (b). Spectra are normalized to the same weight of pellet.

Structural bands and isotopic exchange: In order to investigate the spectral region 600-1250 cm⁻¹ corresponding to the intense

structural bands of zeolite (Si-O and Al-O) the samples were studied after dilution with KBr. Figure 10-A shows the IR spectra of Ti-Beta and Beta samples. The main structural vibration bands characteristic of zeolite-type material are observed at 1225, 1090 and 806 cm⁻¹. Another important and distinctive feature for Ti-Beta is observed at about 955 cm⁻¹. Although the assignment of this band is still in debate, the presence of this band after dehydration of samples under high-vacuum conditions is generally accepted as a solid proof for the incorporation of Ti into the framework [41, 50-53]. This band is notably different from the one at 930 cm⁻¹ that can be observed in zeolite Beta. The latter is assigned to the $\nu(\text{Si-OH})$ vibrations. In order to shed more light on the origin of this band the two samples were subjected to an isotopic H-D exchange. After D₂O exchange, the IR spectra of Ti-Beta and Beta samples (Figures 10-B) show a strong decrease of the bands in the $\nu(\text{OH})$ (3750-3500 cm⁻¹) range with a concomitant formation of a $\nu(\text{OD})$ band (2760-2600 cm⁻¹). Moreover a 20 cm⁻¹ shift of the band at 930 cm⁻¹ is also observed in the pure zeolite sample. This latter is attributed to the H-D exchange of silanol groups [54]. A negligible shift, from 953 cm⁻¹ to 955 cm⁻¹ is observed in the case of plasma treated material. This result undoubtedly confirms the hypothesis of Si-O-Ti formation.

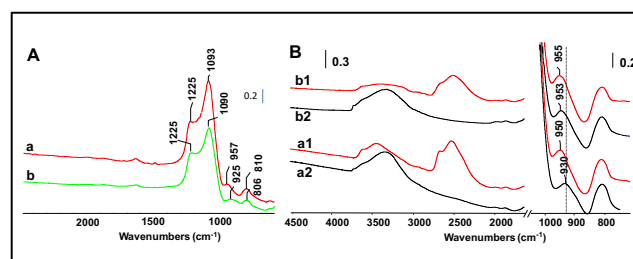


Fig. 10 (A) IR spectra of Ti-Beta (a) and initial zeolite Beta (b) calcined samples diluted in KBr (2 wt.%). (B) IR spectra of Ti-BEA (a) and Beta (b) calcined samples diluted in KBr (5 wt.%) before (1) and after (2) D₂O exchange.

Acidic properties: Pyridine (Py) has been employed as a probe molecule to study the acidity of Beta, Ti-Beta, TiO₂/BEA and TiO₂ samples. Figure 11 presents the recorded IR spectra of these samples after Py adsorption (Py desorption vs temperature is presented in Figures S2-S3 in supporting information). The IR spectrum of zeolite Beta shows distinct bands at 1455, 1490, 1545, 1622 and 1637 cm⁻¹. In the range 1400-1700 cm⁻¹, chemically adsorbed pyridine was revealed by the usual set of bands: i) at 1545 and 1637 cm⁻¹ assigned to pyridinium ion (PyH⁺), ii) at 1455 and 1622 cm⁻¹ related to Lewis bonded pyridine (PyL₁), and iii) the superposition of signals of Lewis and Brønsted adsorbed species at 1490 cm⁻¹ [55-62]. In the case of Ti-Beta sample, the IR spectrum reveals two additional bands at 1448 cm⁻¹ and 1608 cm⁻¹. According to the IR spectrum of pure TiO₂ sample, these bands are assigned to the interaction of Py molecules with Lewis acid sites of titanium oxide nanoparticles incorporated in zeolite Beta. These bands are very weak in the case of TiO₂/Beta which is probably due to the low specific surface area of large TiO₂ aggregates. Thus, the high intensity of these two bands in Ti-Beta demonstrates the high dispersion and

the cluster form of titanium dioxide (Figure 11). These results are in a good agreement with the results obtained by EDS-SEM and HRTEM. On the other hand Py adsorption data do not point out dramatic modification in the acidic properties of Beta after plasma treatment.

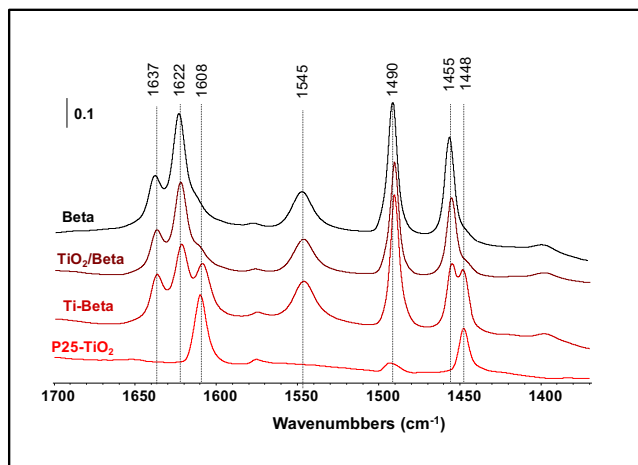


Fig. 11 IR spectra of zeolite Beta, SSD prepared TiO₂/Beta, Ti-Beta and P25-TiO₂ samples after pyridine adsorption (spectra before Py adsorption have been subtracted).

Ti-Beta as photocatalyst: In the present work, methanol photooxidation is used as a model reaction to study the photodegradation of volatile organic compounds (VOCs). No photocatalytic effect has been observed for Beta zeolite sample. The conversion of methanol on Ti-Beta and P25-TiO₂ are presented in Figure 12. Due to the different content of TiO₂ in the two samples, methanol photodegradation rate (V_{MeOH}) has been calculated. It corresponds to the amount of methanol converted (Vol_{MeOH}) per second per gram of TiO₂ (g_{TiO_2}). V_{MeOH} has been calculated with the following formula:

$$V_{\text{MeOH}} = [\text{Vol}_{\text{MeOH-converted}} (\text{ml})] / [m_{\text{TiO}_2} (\text{g}) \times \text{time} (\text{s})] (\text{ml} / g_{\text{TiO}_2} / \text{s}).$$

As shown at Figure 12, a close methanol conversion has been observed using both materials. The photodegradation rates show that V_{MeOH} value obtained using Ti-Beta is 8 times higher than that obtained using P25-TiO₂. This result could be assigned to the high dispersion and accessibility of titanium sites in Ti-Beta that compensate the low TiO_x content in this sample. The higher performance could also be related to the effect of zeolite structure in the separation of the electron/hole charges formed under irradiation, which improves the photocatalytic activity. In addition, the well known acidic properties of Beta zeolite could increase the adsorption of organic compound and hence the photoreactivity.

On the other hand, the selectivity of P25-TiO₂ and Ti-Beta photocatalysts was found to be different. More than 96% photocombustion was obtained in the case of P25-TiO₂, whereas the formation of methyl formate, contributed to ~50% of the photooxidation on Ti-Beta catalysts. Thus the photocombustion reaction contributed to ~50% of the overall transformation on Ti-Beta. As mentioned before the difference in the catalytic activity of bulk TiO₂ is obviously related to the difference of active sites

present in the two materials combined with the impact of zeolite structure in the case of Ti-Beta. These results allow to investigate the use of Ti-Beta for green chemistry applications as the synthesis of methyl formate from methanol using light energy.

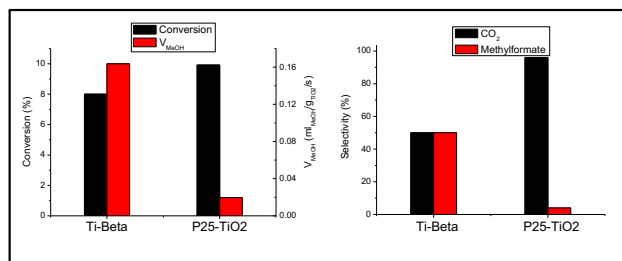


Fig.12 Methanol conversion and CO₂-selectivity during methanol photooxidation on Ti-Beta and P25-TiO₂ photocatalysts vs lamp intensity (%I₀). ([CH₃OH] = 1 % in 20% of O₂ (vol.%) diluted in Ar; flow=25 cm³/min; T=25°C).

Conclusions

Low temperature TiCl₄-plasma was used to incorporate highly dispersed titanium species in the structure of zeolite Beta. The ultimate material was subjected to comprehensive characterization using complementary methods (XRD, NMR, SEM-EDS, IR, UV-visible, and N₂ sorption). More than 50% of the silanol defects present in the zeolite structure were disappeared after TiCl₄-plasma treatment. The formation of chemical bonds "Si-O-Ti" was also revealed. Indeed, the increase of the hexacoordinated aluminum species accompanied with a decrease of the silanol defects pointed out the insertion of Ti into zeolite Beta framework. Pyridine adsorption showed higher dispersion of TiO_x in Ti-Beta sample, which was found 10 times higher than that of TiO₂/Beta prepared by SSD method. The properties of zeolite Beta were not significantly affected after plasma treatment. The parent and the treated samples showed close acidic and adsorption properties. The elaborated Ti-Beta composite was tested as photocatalyst for methanol photooxidation. Plasma prepared Ti-Beta catalysts showed 10 times higher methanol photodegradation rate in respect to the reference P25-TiO₂ catalyst. This result demonstrated the potential of Ti-Beta photocatalysts for applications where the temperature is a critical parameter. It also showed that Ti-Beta could be used for water or air purification, green synthesis or photovoltaic application.

These results open the route to green photochemistry applications of Ti-containing zeolite catalysts prepared by cold plasma method. Regarding the short time of the TiCl₄-plasma treatment, in addition to its efficiency, cost effective and eco-friendly, this method is particularly attractive for commercialization. Furthermore it does not require the use of solvents.

Notes and references

- ^a Laboratoire Catalyse et Spectrochimie, Université de Caen Basse-Normandie, ENSICAEN CNRS, 6 bd Maréchal Juin, 14050 Caen, France
^b Laboratoire de Crystallographie et Science des Matériaux, Université de Caen Basse-Normandie, ENSICAEN CNRS, 6 bd Maréchal Juin, 14050 Caen, France

† Electronic Supplementary Information (ESI) available:
cartographical analysis of Si and Ti in Ti-Beta and SSD TiO₂/Beta
5 samples. Evolution of the IR spectra of Beta and Ti-Beta during Py
desorption under vacuum at different temperature. Bright field TEM
image showing Beta Zeolite -TiO₂ crystals and the corresponding ED
pattern. See DOI: 10.1039/b000000x/

- 10 1 D.F. Ollis, E. Pelizzetti, N. Serpone, *Environ. Sci. Technol.* 1991, **25**, 1522.
2 R.W. Matthews, *J. Phys. Chem.* 1987, **91**, 3328.
3 D. Chatterjee, S. Dasgupta, *J. Photochem. Photobiol. C* 2005, **6**, 186.
4 V. Ramaswamy, N.B. Jagtap, S. Vijayand, D.S. Bhang, P.S. Awati,
15 *Mater. Res. Bull.* 2008, **43**, 1145.
5 J. M. C. Robertson, P. K. J. Robertson, L. A. Lawton, *J. Photochem. Photobiol. A: Chem.* 2005, **175**, 51.
6 S. Romero-Vargas Castrillon, H.I. de Lasa, *Ind. Eng. Chem. Res.* 2007, **46**, 5867.
20 7 B.J. Liu, T. Torimoto, H. Yoneyama, *J. Photochem. Photobiol. A: Chem.* 1998, **113**, 93.
8 J.A. Navio, G. Colon, J.M. Herrmann, *J. Photochem. Photobiol. A: Chem.* 1997, **108**, 179.
9 D. Robert, A. Piscoro, O. Heintz, J.V. Weber, *Catal. Today* 1999, **54**, 291.
25 10 J. Medina-Valtierra, M. Sánchez-Cárdenas, C. Frausto-Reyes, S. Calixto, *J. Mex. Chem. Soc.* 2006, **50**, 8.
11 M. El-Roz, Z. Haidar, L. Lakiss, J. Toufaily, F. Thibault-Starzyk, *RCS adv.* 2013, **3**, 3438.
30 12 H. Hou, H. Miyafuji, S. Saka, *Journal of Materials Science*, 2006, **41**, 8295.
13 J. M. Herrmann, J. Matos, J. Disdier, C. Guillard, J. Laine, S. Malato, J. Blanco, *Catal. Today* 1999, **54**, 255.
14 A. Corma, M.A. Cambor, P. Esteve, A. Martínez, J. Pérez-Pariente, *J. Catal.* 1994, **145**, 151.
35 15 K. Lin, L. Wang, F. Meng, Z. Sun, Q. Yang, Y. Cui, D. Jiang, *J. Catal.* 2005, **235**, 423.
16 M. Lafjah, F. Djafri, A. Bengueddach, N. Keller, V. Keller, *Journal of Hazard. Mater.* 2011, **186**, 1218.
40 17 V. Durgakumari, M. Subrahmanyam, V. Subbaraok, A. Ratnamala, M. Noorjahan, K. Tanaka, *Applied catalysis. A: General* 2002, **234**, 155.
18 S. Anandan, M. Yoon *J. Photochem. Photobiol. C* 2003, **4**, 5.
[19] N. Takeda, T. Torimoto, S. Sampath, S. Kuwabata, H. Yoneyama, *J. Phys. Chem.* 1995, **99**, 9986.
45 20 C. Anderson, A. Bard, *J. Phys. Chem. B* 1997, **101**, 2611.
21 M. Mahalakshmi, S. Vishnu Priya, B. Arabindoo, M. Palanichamy, V. Murugesan, *J. Hazard. Mater.* 2009, **161**, 336.
22 A. Corma, *Chem. Rev.* 1997, **97**, 2373.
23 M. V. Phanikrishna Sharma, K. Lalitha, V. Durga Kumari, M. Subrahmanyam, *J. Hazard. Mater. Sol. Cells* 2008, **92**, 332.
50 24 M. V. Phanikrishna Sharma, K. Lalitha, V. Durga Kumari, M. Subrahmanyam, *J. Hazard. Mater.* 2008, **160**, 568.
25 M.V. Phanikrishna Sharma, K. Lalitha, V. Durga Kumari, M. Subrahmanyam, *Chemosphere* 2008, **72**, 644
55 26 M. Álvaro, E. Carbonell, P. Atienzar, H. García, *PCCP*, 2006, **7**, 1996.
27 M. V. Shankar, K.K. Cheralathan, B. Arabindoo, M. Palanichamy, V. Murugesan, *J. Mol. Catal. A: Chem.* 2004, **223**, 195.
28 M. P. Reddy, H.H. Phil, M. Subrahmanyam, *Catal. Lett.* 2008, **123**, 56.
60 29 M. Takeuchi, J. Deguchi, M. Hidaka, S. Sakai, K. Woo, P.P. Choi, J.K. Park, M. Anpo, *Appl. Catal. B: Environ.* 2009, **89**, 406.
30 J.-P. Nogier, Y. Millot, P.P. Man, C. Méthivier, M. Che, S. Dzwigaj, *Catal Lett* 2009, **130**, 588
31 N. G Kubala, C. Rowlette, C.A. Wolden, *J. Phys. Chem.* 2009, **113**, 16307.
65 32 X. L. Zhang, L.H. Nie, Y. Xu, C. Shi, X.F. Yang, A.M. Zhu, *J. Phys. D: Appl. Phys.* 2007, **40**, 1763.
33 C. Jiménez, D. D. Barros, A. Darraz, J.L. Deschanvers, L. Rapenne, P. Chaudouët, J. E Méndez, F. Weiss, M. Thomachot, T. Sindzingre, G. Berthomé, F. J. Ferrer., *Surf. & Coat. Techn.* 2007, **201**, 8971.
70 34 P. C. Rowlette, C.A. Wolden, *App. Mat. & Interf.* 2009, **11**, 2586.
35 M. El-Roz, L. Lakiss, V. Valtchev, S. Mintova, F. Thibault-Starzyk, *Mesopor. Micropor. Mater.*, 2012, **158**, 148.
36 M. El Roz, P. Bazin, F. Thibault-Starzyk, *Catal. Today*, 2013, **205**, 111.
75 37 M. El-Roz, K. Monika, Pegie Cool, F. Thibault-Starzyk, *J. Phys. Chem. C*, 2012, **116**, 13252.
38 M. El-Roz, A. Vicente, K. Bozhilov, F. Thibault-Starzyk, V. Valtchev, submitted.
80 39 R. Matero, A. Rahtu, M. Ritala *Chem. Mater*, 2001, **13**, 4506.
40 J. Yan, G. Gan, J. Du, J. Sun, *J. Phys.: Conf. Ser.* 2009, **152**, 1.
41 W. Fan, R.-G. Duan, T. Yokoi, P. Wu, Y. Kubota, T. Tatsumi, *J. Am. Chem. Soc.* 2008, **130**, 10150.
42 Y. Cheneviere, F. Chieux, V. Caps, A. Tuel, *J. Catal.* 2010, **269**, 161.
85 43 O. I. Micic, M. Meglic, D. Lawless, D. K. Sharma, N. Serpone *Langmuir* 1990, **6**, 4403.
44 N. Serpone, D. Lawless, R. Khairutdinov, *J. Phys. Chem. B* 1995, **99**, 16646.
45 S. Turner, O.I. Lebedev, F. Schröder, D. Esken, R. A. Fischer and G. Van Tendeloo *Chem. Mater* 2008, **20**, 5622.
90 46 A. Vimont, F. Thibault-Starzyk, J. C. Lavalley, *J. Phys. Chem. B* 2000, **104**, 286.
47 F. Thibault-Starzyk, A. Vimont, J.-P. Gilson, *Catal. Today* 2001, **70**, 227.
95 48 A. Vimont, F. Thibault-Starzyk, J. C. Lavalley, *Stud. Surf. Sci. Catal.* 2000, **130**, 2963.
49 J.-P. Gallas, J.-M. Goupil, A. Vimont, J.-C. Lavalley, B. Gil, G.- P. Gilson, O. Miserque, *Langmuir* 2009, **25**, 5825.
50 G. Ricchiardi, A. Damin, S. Bordiga, C. Lamberti, G. Spano, F. Rivetti, A. Zecchina, *J. Am. Chem. Soc.* **2001**, *123*, 11409-11419.
100 51 D. R. C. Huybrechts, Ph. L. Buskens, P. A. Jacobs, *J. Mol. Catal.* 1992, **71**, 129.
52 M. A. Cambor, A. Corma, J. Perez-Pariente, *J. Chem. Soc. Chem. Commun.* 1993, 557.
105 53 M. R. Boccuti, K. M. Rao, A. Zecchina, G. Leofanti, G. Petrini, *Stud. Surf. Sci. Catal.* 1989, **48**, 133.
54 G. Bellussi, A. Carati, G. M. Clerci, G. Maddellini, R. Millini, *J. Catal.* 1992, **133**, 220.
55 A. Vimont, F. Thibault-Starzyk, J. C. Lavalley, *J. Phys. Chem. B* 2000, **104**, 286.
110 56 F. R. J. Cannings, *Phys. Chem.* 1968, **72**, 4691.
57 M. Lefrançois, G. J. Malbois, *Catal.* 1971, **20**, 350.
58 R. Buzzoni, S. Bordiga, G. Ricchiardi, C. Lamberti, A. Zecchina, G. Bellussi, *Langmuir* 1996, **12**, 930.
115 59 T. Barzetti, E. Selli, D. Moscotti, L. Forni, *J. Chem. Soc., Faraday Trans.* 1996, **92**, 1401.
60 J. R. Sohn, E. H. Park, *J. Ind. Eng. Chem.* 2000, **6**, 312.
61 A. Satsuma, A. Hattori, K. Mizutani, A. Furuta, A. Miyamoto, T. Hattori, Y. Murakami, *J. Phys. Chem.* 1988, **92**, 6052.
120 62 J. R. Sohn, J. Kim, T.-D. Kwon, E. H. Park, *Langmuir* 2002, **18**, 1666.